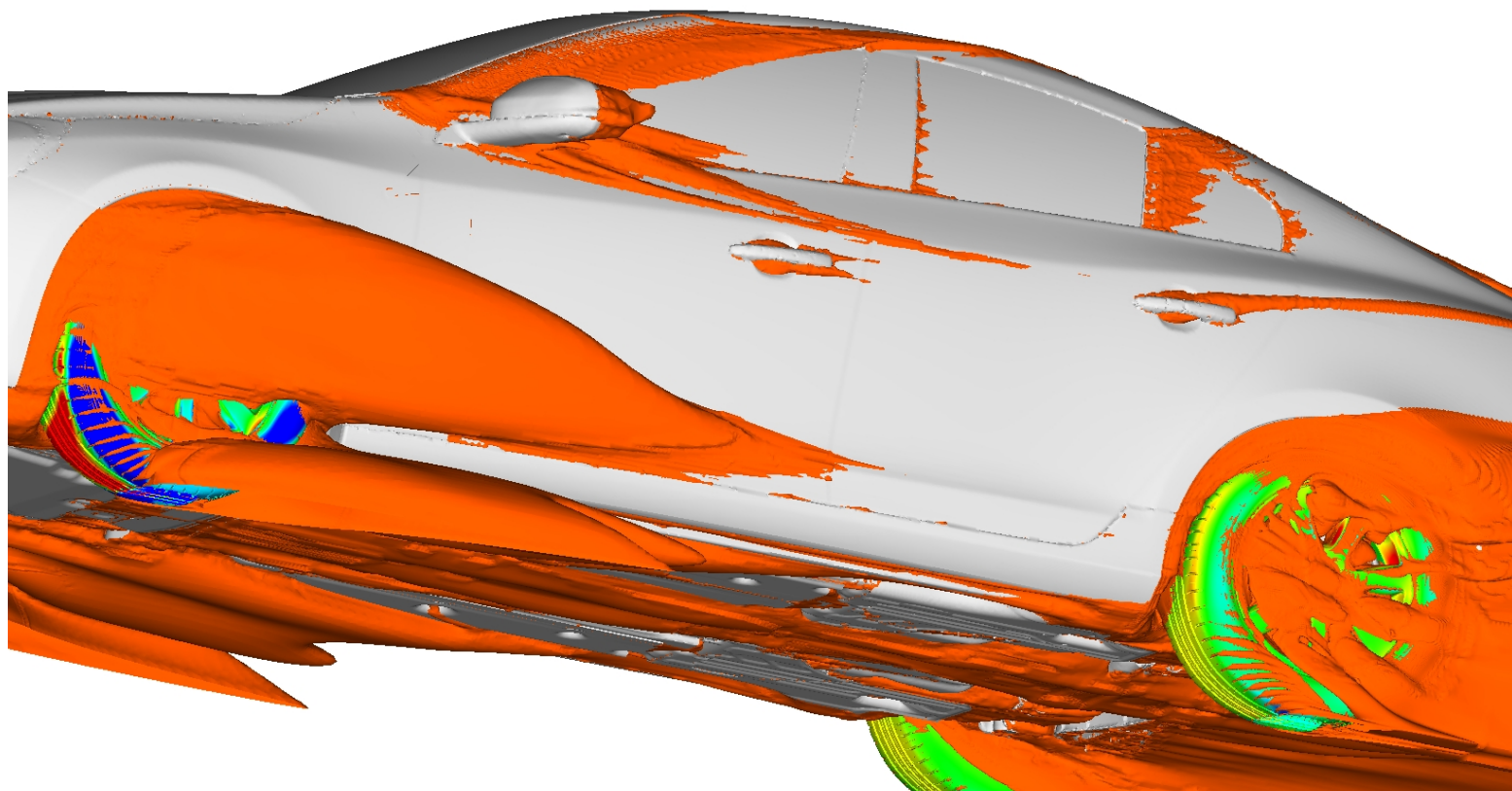


# CHALMERS



## Investigation of Tyre Geometry Influence on Road Vehicle Aerodynamics

*Master's Thesis in Automotive Engineering*

Teddy Hobeika

Department of Applied Mechanics

*Division of Vehicle Engineering and Autonomous Systems*

*Road Vehicle Aerodynamics Group*

CHALMERS UNIVERSITY OF TECHNOLOGY

Gothenburg, Sweden 2012

Master's Thesis 2012:47



MASTER THESIS IN AUTOMOTIVE ENGINEERING

Investigation of Tyre Geometry Influence on Road Vehicle  
Aerodynamics

Teddy Hobeika

Department of Applied Mechanics  
*Division of Vehicle Engineering and Autonomous Systems*  
*Road Vehicle Aerodynamics Group*  
CHALMERS UNIVERSITY OF TECHNOLOGY  
Göteborg, Sweden 2012

Investigation of Tyre Geometry Influence on Road Vehicle Aerodynamics

Teddy Hobeika

© Teddy Hobeika, 2012

Master's thesis in Automotive Engineering 2012:47

ISSN 1652-8557

Department of Applied Mechanics

Division of Vehicle Engineering and Autonomous Systems

Road Vehicle Aerodynamics Group

Chalmers University of Technology

SE-412 96 Göteborg

Sweden

Chalmers Reproservice  
Göteborg, Sweden 2012

## Abstract

Wheels aerodynamics and its effect on vehicle aerodynamics have been the focus of several papers in the automotive industry. This report focuses mainly on the effects of tyre geometry on road vehicle aerodynamics using Computational Fluid Dynamics (CFD) simulations. The tyres, obtained from the manufacturer as geometry files, were deformed based on measured wind tunnel data of the same tyres under similar load and rotating at 100 kph. The tyre deformation preserved a certain contact patch which was measured at stationary position. The main tyre comparisons included comparison of tyre profiles, different tyre patterns, and different combinations of pattern features of the same tyre. Some configurations were evaluated with different rims to investigate the rim dependency of the results. As the simulations used Moving Reference Frame (MRF) approach then some configurations were also evaluated with the same rim having two different spoke positions. The different pattern features investigated were: Main grooves, side grooves, and edge pattern. The main grooves gave the most consistent results of a few drag counts reduction in drag and lift. The different tyre profiles also showed different magnitudes of drag and lift reduction. The side groove showed an increase in drag in all open rim cases but with the magnitude dependent on the rim. The edge pattern however showed no clear trend although when different combinations of the above features were performed a strong interaction could be seen between the side grooves and the edge pattern. The presence of both showed a consistent increase in drag and lift with the magnitude of the increase being rim dependent. This increase in drag can be clearly seen in the flow field as strong vortices generated at the front wheels due to both the edge pattern and the side grooves. Simulations also showed that the edge pattern had a bigger increase in drag on a sports wagon than on a sedan as having the edge pattern on the rear wheels have shown a drop in base pressure due to the interaction of the tyre vortices with the rear wake. The comparison of two different tyres showed a reduction in drag dependent on the spoke position. It is worth noting that the main difference between Tyres 1 and 2 is the absence of the side groove on Tyre 2 as they both have a very similar tyre profile. The reduction in drag between Tyre 1 and 2 has been replicated in the wind tunnel on one of the rims.

## Acknowledgments

I'd like to thank:

Dr. Simone Sebben, my supervisor at Volvo Car Corporation for her constant guidance and support throughout my thesis.

Dr. Lennart Lofdahl, my examiner at Chalmers University of Technology, for giving me the opportunity to perform such a thesis at Volvo Car Corporation.

Dr. Christoffer Landstrom for his valuable input and guidance as this thesis comes within his PhD thesis area of wheel aerodynamics.

Mats Beckman, tyre development engineer at Wheels and Tyres department at Volvo Car Corporation, for his support with tyre models and data.

Volvo CFD group, a.k.a CFD Familje, for showing outstanding patience and friendliness in answering all my questions related to the use and scripting of different softwares and computer programs; for all the outings and Fikas we shared together.

My family, for their love and support; for helping me become the engineer I am today.

Teddy Hobeika, Gothenburg August 27 2012

# Contents

<b>1</b>	<b>Introduction</b>	<b>1</b>
1.1	Background Information . . . . .	2
1.2	Objective . . . . .	2
1.3	Methodology . . . . .	3
1.3.1	Theory . . . . .	3
1.3.2	Numerical Setup . . . . .	4
<b>2</b>	<b>Configurations</b>	<b>6</b>
2.1	Tyre Deformation . . . . .	7
2.2	Deformation1 vs. Deformation2 . . . . .	8
2.3	Tyre Profiles . . . . .	8
2.4	Pattern Features . . . . .	9
2.5	Rim Configurations . . . . .	11
2.6	Car configurations . . . . .	12
2.7	T1 vs. T2 . . . . .	13
<b>3</b>	<b>Results</b>	<b>14</b>
3.1	Deformation 1 vs. Deformation 2 . . . . .	15
3.2	Tyre Profiles . . . . .	17
3.3	Tyre features . . . . .	18
3.3.1	Main Grooves . . . . .	18
3.3.2	Side Grooves . . . . .	19
3.3.3	Edge Pattern . . . . .	21
3.3.4	Main and Side Grooves . . . . .	23
3.3.5	Main Grooves and edge pattern . . . . .	24
3.3.6	Side Grooves and edge pattern . . . . .	25
3.3.7	Full Pattern . . . . .	26
3.4	Sedan vs. Sportswagen . . . . .	29
3.5	T1 vs. T2 . . . . .	30

<b>4 Summary</b>	<b>32</b>
4.1 Limitations . . . . .	33
4.2 Conclusions . . . . .	34
4.3 Recommendations . . . . .	35
4.4 Future Work . . . . .	35
<b>Bibliography</b>	<b>37</b>

# 1

## Introduction

This chapter gives a general overview of the purpose of this masters thesis as well as the methods used to complete the work. The brief background information section gives a general explanation of the applicability of the thesis work to real life and some previous work done in the field. The methodology section describes the basics of the simulations' physical resemblance and setup.

## 1.1 Background Information

For several years now, sustainability and energy efficiency have become a major area of research and development for the automotive industry. With stricter regulations and tax rates being introduced every year on CO2 emissions and fuel consumption, car manufacturers are pushed into seeking solutions that do not compromise their cars' performance. Aerodynamics is one of the several fields where such solutions are pursued.

Road vehicle aerodynamics is the study of how air resistance affects a vehicle's handling. On passenger cars at zero yaw angle air resistance can be simplified into two major forces: drag and lift. Drag is the force that resists the car's forward motion as a result of the pressure differences in front and behind the car. The drag of a vehicle is usually represented as a dimensionless number known as Drag Coefficient ( $C_d$ ).  $C_d$  is a dimensionless parameter used to describe how good a car's aerodynamic performance is. When representing the sum of forces acting on a vehicle shown in equation 1.1, aerodynamic drag is represented in equation 1.2 thus having a direct effect on fuel consumption.

$$F_{drive} = F_{drag} + F_{acceleration} + F_{rollingresistance} + F_{gradeability} \quad (1.1)$$

$$F_{drag} = 1/2\rho v^2 C_D A \quad (1.2)$$

$$F_{lift} = 1/2\rho v^2 C_L A \quad (1.3)$$

Lift however is the force exerted on the car in the vertical direction as a result of the pressure difference above and underneath the car. It is usually represented as a dimensionless number too known as Lift Coefficient ( $C_l$ ) and shown in equation 1.3.  $C_l$  also influences fuel consumption through influencing the car's rolling resistance. However for passenger cars this effect is negligible due to low  $C_l$  figures although it becomes much more pronounced in the motor sport industry.  $C_l$  can however have a significant effect on vehicle handling at high speeds.

The car's wheels and wheelhouses contributes to more than 30 % of the vehicle drag is due to the wheels' rotation [1]. The wheels, being rotating, tend to put energy in the form of vortices into the flow thus affecting the under body flow structure and eventually the resultant drag. Different rim designs and tyres have shown a difference in the vehicle's overall drag in wind tunnel tests as well as in Computational Fluid Dynamics (CFD) simulations. [2, 3, 4, 5, 6, 7, 8, 9] .

## 1.2 Objective

The objective of this thesis is to furthermore investigate the effect of tyre profile and pattern on the drag and lift of a vehicle. The aim of which is understanding the drag contribution of different tyre features in CFD and what to take into consideration when performing simulations.

## 1.3 Methodology

### 1.3.1 Theory

In order to simulate the flow behavior the flow needs to be describes in a mathematical form. This form includes three governing equations: the continuity equation, the mass conservation equation and the energy conservation equation; respectively equations 1.4, 1.5, and 1.6.

$$\frac{\partial \rho}{\partial t} + \frac{\partial \rho u_i}{\partial x_i} = 0 \quad (1.4)$$

$$\frac{\partial \rho u_i}{\partial t} + \frac{\partial \rho u_i u_j}{\partial x_j} = -\frac{\partial p}{\partial x_i} + \frac{\partial \tau_{ij}}{\partial x_j} + \rho f_i \quad (1.5)$$

$$\frac{\partial \rho E}{\partial t} + \frac{\partial \rho u_j E}{\partial x_j} = -\rho q + \frac{\partial}{\partial x_j} \left( k \frac{\partial T}{\partial x_j} \right) - \frac{\partial u_i p}{\partial x_j} + \frac{\partial u_i \tau_{ij}}{\partial x_j} + \rho f_i u_i \quad (1.6)$$

where  $E = e + \frac{V^2}{2}$  and  $p = \rho RT$ .

As for automotive application purposes, speeds at which simulations are run do not exceed  $0.3Mach$  then the flow can be assumed incompressible with  $\rho$  being constant. And as the issue at hand here does not involve heat transfer or temperature changes then the flow can also assumed to be isothermal, thus the energy equation does not need to be solved. Thus the continuity and mass conservation equations are simplified to the form present in equations 1.7 and 1.8.

$$\frac{\partial u_i}{\partial x_i} = 0 \quad (1.7)$$

$$\rho \frac{\partial u_i u_j}{\partial x_j} = -\frac{\partial p}{\partial x_i} + \frac{\partial \tau_{ij}}{\partial x_j} + \rho f_i \quad (1.8)$$

where the viscous stress tensor  $\tau_{ij} = 2\mu S_{ij}$  in which the strain rate tensor  $S_{ij} = \frac{1}{2} \left( \frac{\partial u_i}{\partial x_j} + \frac{\partial u_j}{\partial x_i} \right)$

Now using the Reynolds-Averaged Navier-Stokes approach, the velocity and pressure terms are decomposed into a time-averaged part and a dependent fluctuating part which when replaced into the governing equations give equations 1.9 and 1.10

$$\frac{\partial \bar{U}_i}{\partial x_i} = 0 \quad (1.9)$$

$$\rho \bar{U}_j \frac{\partial \bar{U}_i}{\partial x_j} = -\frac{\partial \bar{P}}{\partial x_i} + \frac{\partial}{\partial x_j} \left( \mu \frac{\partial \bar{U}_i}{\partial x_j} - \rho \bar{u}_i u_j \right) \quad (1.10)$$

### 1.3. METHODOLOGY

---

Now using the Boussinesq assumption the Reynolds stresses can be written in terms of eddy viscosity  $\mu_t$  which is modeled as  $\rho C_\mu \frac{k^2}{\varepsilon}$ . This is how the turbulent kinetic energy,  $k$ , and the turbulence dissipation rate,  $\varepsilon$ , are introduced into the governing equations in the realizable  $k - \varepsilon$  turbulence model.

This model however cannot be applied all the way down to the wall so a wall function has to be used at the wall. The standard wall function, which is the one used in this thesis, defines the near wall velocity,  $U^+$ , as a function of the non-dimensional wall distance,  $y^+$ , as shown in equation 1.11

$$U^+ = \frac{1}{\kappa} (E y^+) \quad (1.11)$$

where  $\kappa = 0.4187$ , von Karman constant, and  $E = 9.793$ , Empirical constant.

#### 1.3.2 Numerical Setup

The above objective was mainly achieved using CFD simulations at Volvo Car Corporation(VCC). The simulations used a sedan and a sports-wagon model, as well as different rim designs, provided by VCC. The simulation process followed the VCC AEDCAE02 procedure for running open cooling CFD simulations.

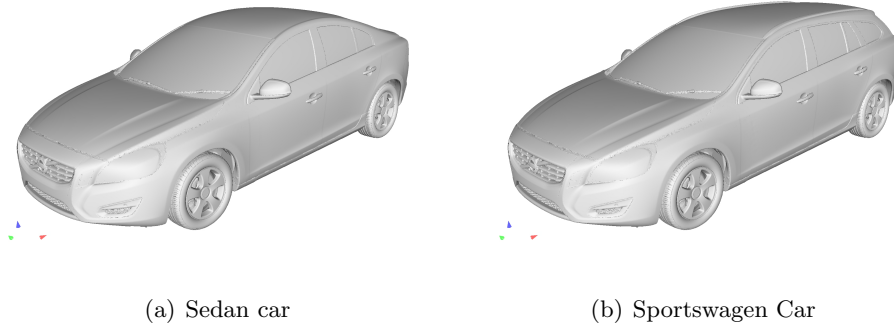


**Figure 1.1:** Cars used in simulations

The CAD cleaning of the models, which were fully detailed production models, was done in ANSA. A volume mesh was created in Harpoon from an ANSA surface mesh and fluent was used to solve the flow field. Realizable k-epsilon turbulence model was used with a standard wall function and second order discretization for momentum equations. Moving Reference Frame (MRF) boundary conditions were applied in order to achieve correct boundary condition on the rim spokes at the expense of introducing some numerical error in the form of a pressure gradient in the volume to which it is applied.

### 1.3. METHODOLOGY

---

Simulations were run at 100 kph with 0.1 % inlet turbulent intensity. The vehicle surface meshing ranged from 1.25 to 5 mm thus keeping a  $y$  plus value mostly between 30 and 300. The cases usually were between 110 to 120 million cells with refinement boxes placed around the sensitive regions of the car to limit mesh growth for a better flow resolution. The mesh resolution and refinement boxes of course are limited by the processing and computational power available as usual. Figure 1.2 shows the mesh refinements in a longitudinal plane located at the middle of the car ( $y=0$  plane).

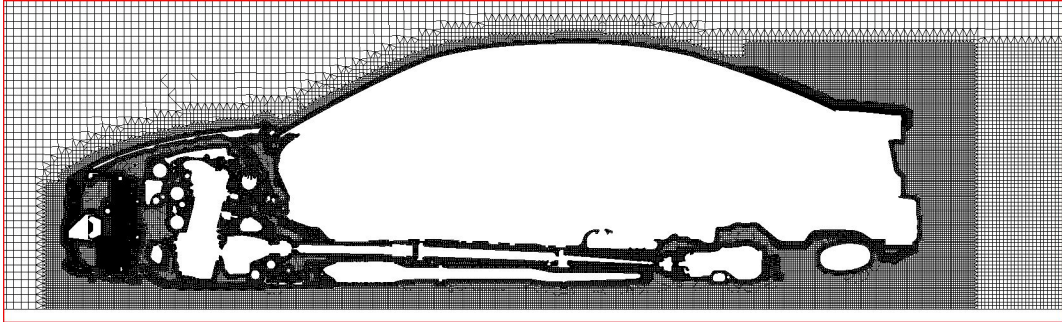


**Figure 1.2:** A clip of the mesh at the  $y=0$  plane.

As the area of interest was the tyre a mesh of 1.25 mm was used to accurately resolve the tyre geometry and a slow expansion into the fluid was used in order not to dampen the vortices generated as they transition to a coarser mesh resolution. Mesh refinement and solver boundary conditions were preserved throughout all the configurations in order to keep the results comparable.

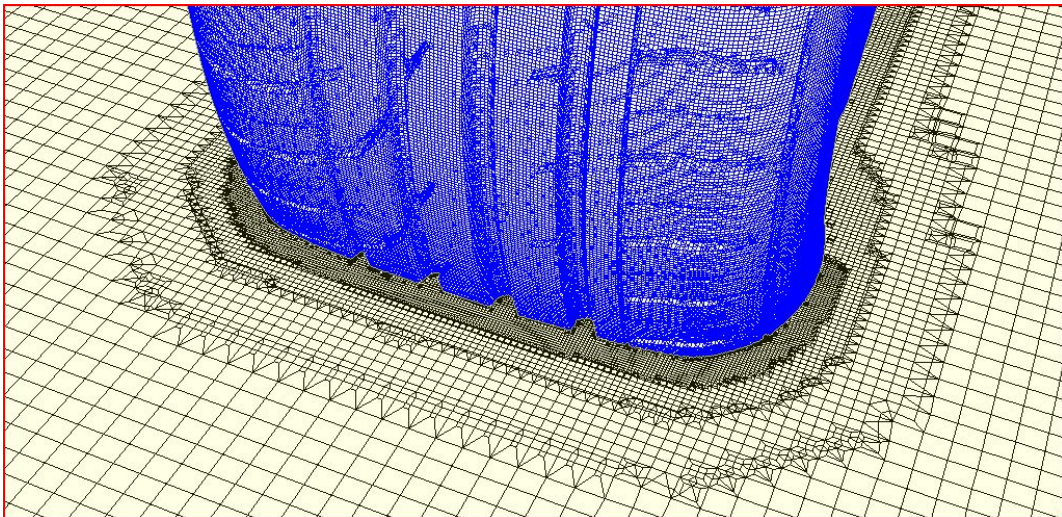


**Figure 1.3:** the surface mesh of the tyre (blue wireframe) as well as the expansion of the mesh into the fluid (black wireframe).

# 2

## Configurations

This chapter describes the different configurations simulated and some of the reasons why these specific configurations were done. A number of terms will be introduced with a coding in order to distinguish the configurations from one another. The coding will make it quite simpler to compare the different configurations later in the results section.

## 2.1 Tyre Deformation

As the tyre deforms under the weight of the car then the tyre CAD which is originally perfectly round needs to be morphed in ANSA to replicate the correct tyre shape after loading. However one must keep in mind that the tyre in the simulation is expected to be rotating at a speed of 100 kph and not stationary. Previous work by Landström et al.[7], has described and measured the deformations of the tyre due to centrifugal forces from wheel rotation. Two sets of measurements on two different tyres where done and for the purpose of this investigation an average of both tyre deformations was used as the differences between the deformations were not large at 100 kph. The deformations presented in [7] are shown in figure 2.1.

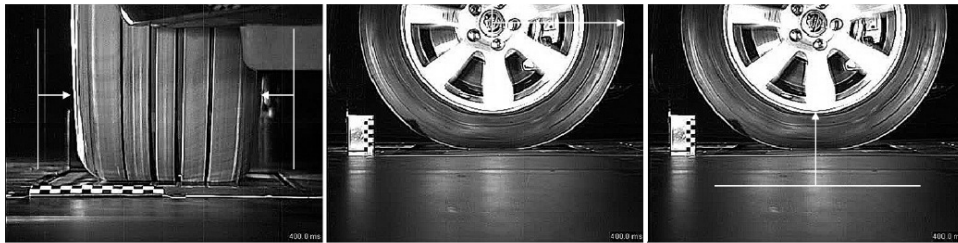


Figure 13 Definitions of tyre deformation measurements. Left: Axial compression, Centre: Radial expansion, Right: Vertical lift.

Figure 2.1: Wheel deformations as presented by Landström[7]

The morphing of the tyre also preserved a contact patch area measured on a real tyre at stationary position on the same car as previous studies on this have shown the importance of replicating realistic contact patch area in the simulations [10, 11].

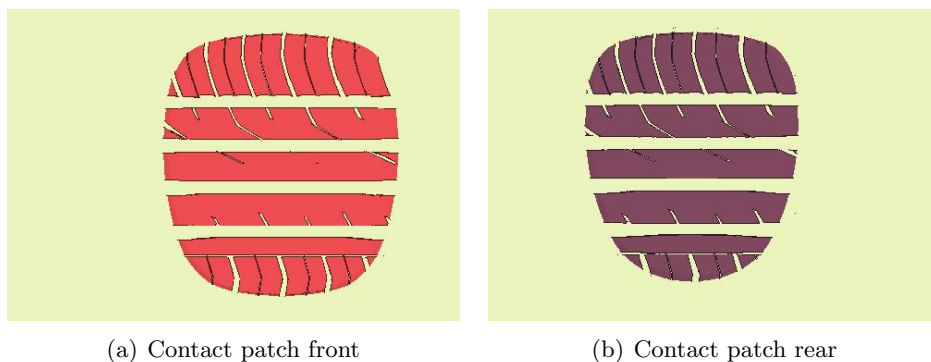


Figure 2.2: The differences between the contact patches

## 2.2 Deformation1 vs. Deformation2

At the very beginning of this work, a comparison between two different sets of deformations was performed: Def1 and Def2.

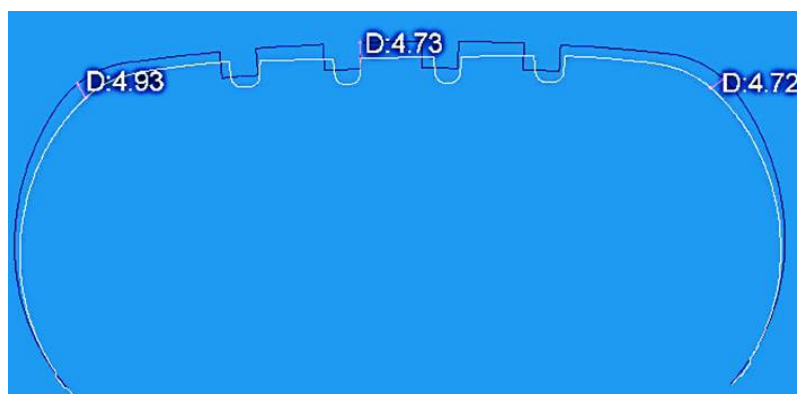
Def1 is the general morphing applied on a slick tyre for CFD purposes at VCC. The tyre lift, axial contraction, and radial expansion deformations have standard values as recommended in [10]. Also when adding details on the belt section these details tend to be unpreserved at the contact patch. The most notable difference being when adding rain grooves (called main grooves in this thesis) on the tyre, these grooves tend to be cut at the ground while they are expected to continue through. These grooves are there mainly to allow water through, however, in the absence of water these grooves would actually be allowing air through.

Def 2 was then developed in order to preserve the tread details and especially the main grooves at the contact patch. Def 2 also used the measured data from [7] for the different tyre deformations in order to get it as close as possible to a real tyre shape.

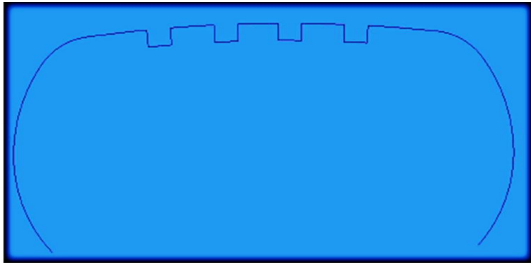
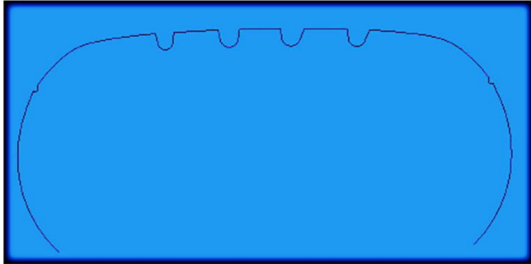
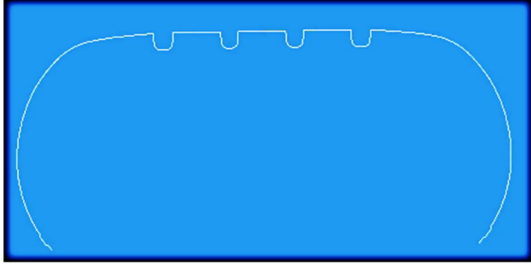
Note that all deformations after this investigation were done according to def2. A comparison of the two deformations will be presented in section 3.1

## 2.3 Tyre Profiles

The tyre profile expression used in throughout this thesis stands for the inflated section drawing of the tyre. At early stages of a car project, the tyre profiles are not available. Then, it is common to have standard tyres to be used for running CFD simulations. The profile of such a tyre will be called “Generic” tyre. One of the goals of this thesis was to check different tyre profiles and their effect on lift and drag. Along with the generic tyre profile two real production tyre profiles were investigated. However the two production tyres had very similar profiles so only one of them was simulated for comparison with the Generic tyre. The coding for the different tyre profiles will follow table 2.1 while figure 2.3 shows the differences between a Generic and a real production tyre profile.



**Figure 2.3:** Picture showing the differences between the two profiles. Distances in mm

Code	Tyre Name	Profile Curve
G	Generic	
T1	Tyre 1	
T2	Tyre 2	

**Table 2.1:** Rim Configurations and Coding

## 2.4 Pattern Features

Three main pattern features were identified for this study: Main grooves, side grooves, and edge pattern. All three are shown in the figure 2.4 each separately on a slick tyre.

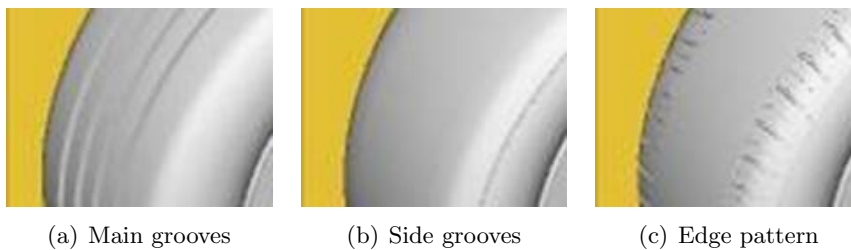


**Figure 2.4:** The three tyre features investigated

## 2.4. PATTERN FEATURES

A total of 8 different combinations can be evaluated with these features following Table 2.2. A coding has been used to identify these combinations. The coding system follows the logic principal of combinations while preserving the following order: main grooves, side grooves, and edge pattern. This coding is also present in Table 2.2.

Code	Tyre Features			Picture
	Main Grooves	Side Grooves	Edge Pattern	
000				
100	✓			
010		✓		
001			✓	
101	✓		✓	
110	✓	✓		
011		✓	✓	
111	✓	✓	✓	

**Table 2.2:** Tyre Pattern Coding

## 2.5 Rim Configurations

The tyre and rim are both rotating together and the flow crossing over the tyre has a strong interaction with the flow going through the rim. Therefore, several rim designs had to be investigated in order to evaluate the rim dependency of the different combinations. Two rim designs were used for this study with a variation on each thus leading to four rim designs in total. The Creon rim show in table 2.3 has been rotated by 36 degrees in order to invert the spoke's position. A similar investigation had been done by Landström et al.[2] which showed a dependency of the flow on spoke position especially for thick spokes. The Oden rim also presented in table 2.3 has been closed by a flat plate on the outer most section of the rim in order to simulate a closed rim. The rims and their respective coding are presented in table 2.3

Code	Rim Name	Picture
C	Creon	
CR	Creon Rotated	
O	Oden	
F	Flat	

**Table 2.3:** Rim Configurations and Coding

## 2.6 Car configurations

A couple of simulations were also run on a sportswagon in order to investigate the sensitivity of the tyre changes to car shapes. The sportswagon and sedan both share the same platform so the wheel positions, underbody and engine bar were identical however with a notable difference on the exterior and rear end shape as can be seen in figure 2.5. The configurations ran on the sportswagon all used T1 profile and Creon rim. Only four tyre pattern configurations were tested being 000, 100, 101, and 111, according to table 2.1

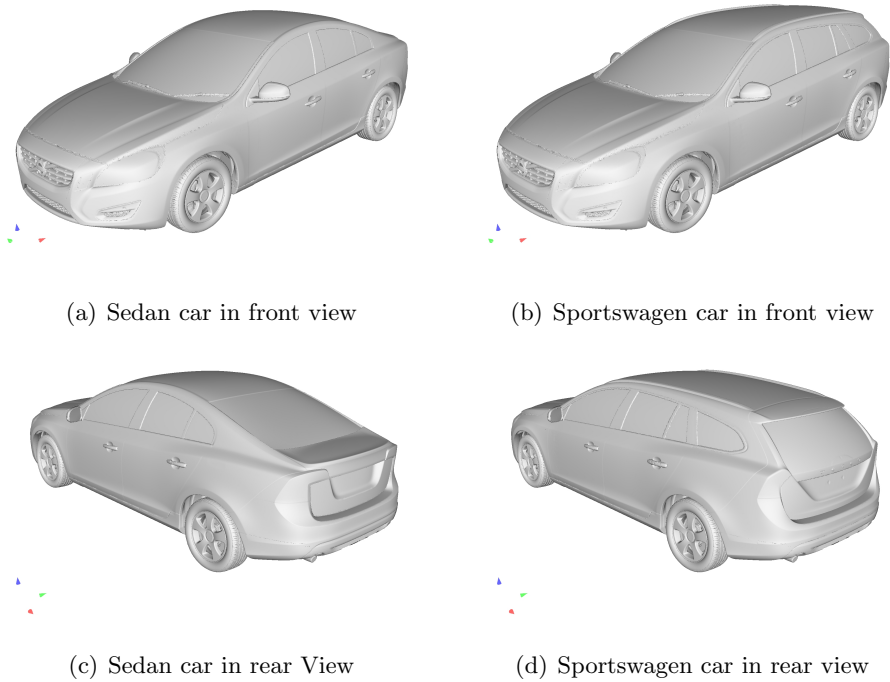


**Figure 2.5:** Comparison of the different cars

## 2.7 T1 vs. T2

T1 and T2 are tyres with almost identical profiles and four rain grooves of approximately the same size. The biggest difference between the two tyres is the pattern itself with T2 having no side groove and a smoother edge pattern. Both these tyres are investigated on the Oden, Creon, and Creon Rotated rims. Figure 2.6 shows both tyres.

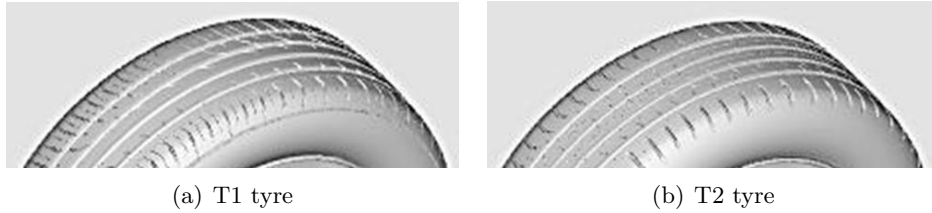


**Figure 2.6:** Comparison of both T1 and T2 tyres

# 3

## Results

**T**his chapter presents the results of the different configurations simulated. It includes a detailed explanation and comparison of these results.

### 3.1 Deformation 1 vs. Deformation 2

As expected there were differences in aerodynamic forces between deformations 1 and 2 for slick tyres. However the biggest difference was observed when a grooved tyre was used. The results are summarized in table 3.1.

Tyre Config.	Drag		Lift	
	Def.1	Def.2	Def.1	Def.2
Slick	0	3	0	10
Grooved	6	-1	9	-14
$\Delta$	6	-4	9	-24

**Table 3.1:** All values are count differences to Def.1 slick (used as reference). However the Delta (last) row shown the difference of going from Slick to Grooved for each deformation.

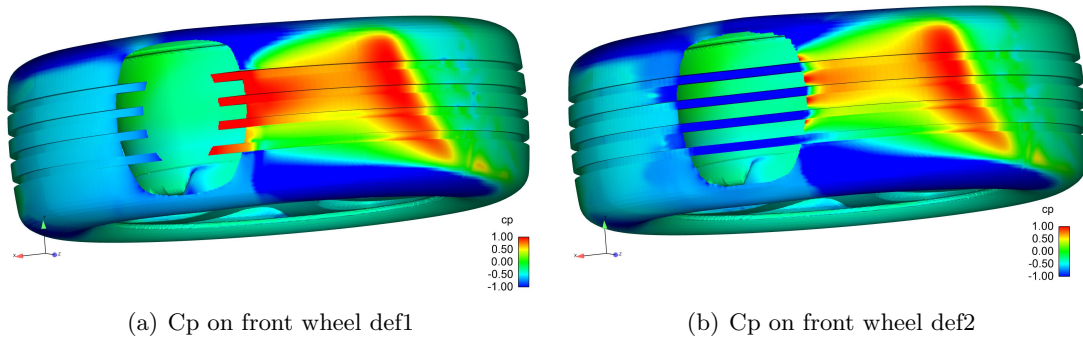


**Figure 3.1:** Comparison of Cp plots between def1 and def2 on front wheels

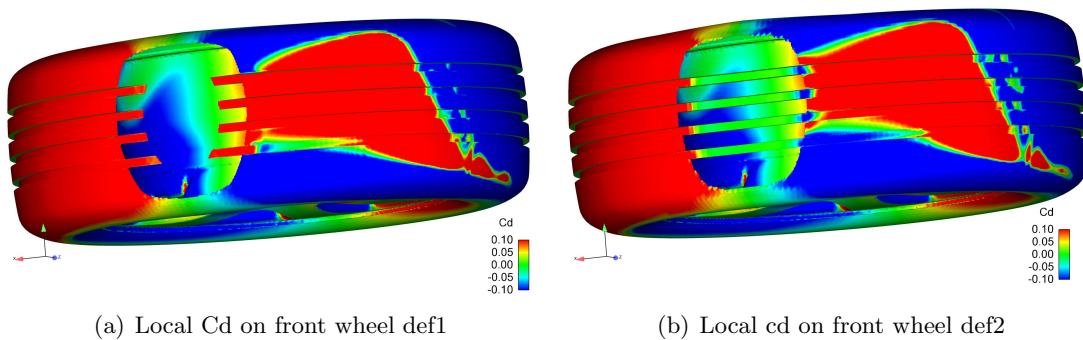
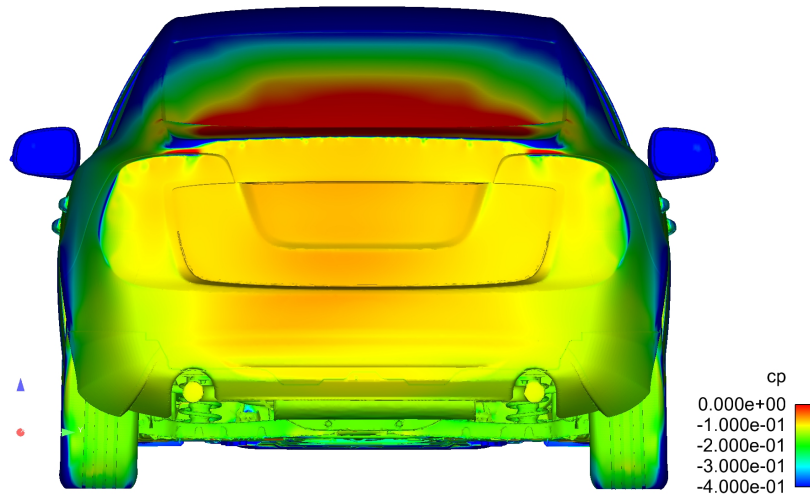


**Figure 3.2:** Comparison of local Cd plots between def1 and def2 on front wheels

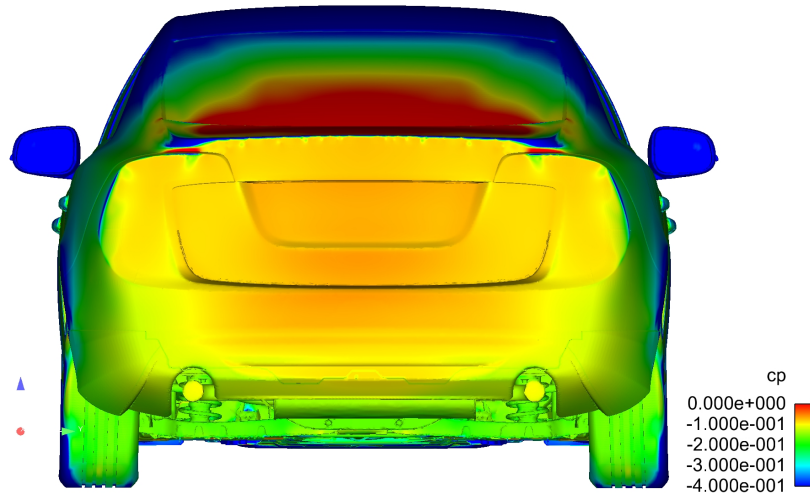
### 3.1. DEFORMATION 1 VS. DEFORMATION 2

---

Figures 3.1 and 3.2 show the difference between having the main grooves cut at the contact patch or connected and their effect on pressure distribution and the local drag on the tyre itself. Note that the figure only shows the effect on the tyre itself although the flow field around it also changes affecting different parts of the car as well. An increase in base pressure could also be seen without much effect on the rear wake structure as the grooves also diminish the jetting effect on the rear wheels and allowing air through slightly reduces the wake. The effect on base pressure can be seen in figure 3.3.



(a) Base pressure plot of def1



(b) Base pressure plot of def2

**Figure 3.3:** Comparison of base pressure plots between def1 and def2

### 3.2 Tyre Profiles

The tyre profiles compared are the generic and tyre 1, G and T1 respectively. The results are present in table 3.2.

Grooved-Slick Rim Config.	Drag		Lift	
	Generic	Tyre 1	Generic	Tyre 1
Creon	-4	-1	-24	-12
Oden	-3	-3	-19	-15

**Table 3.2:** All values are count differences between the grooved and slick tyres of each configuration respectively.

Adding the rain grooves to a slick tyre seems to give a persistent trend of slight drag reduction between 1 to 4 counts and a lift reduction between 12 to 24 counts. The differences in drag between the different rim designs are close to the uncertainty of CFD. However, looking at the profile differences, the generic tyre shows a bigger reduction in both drag and lift than the T1 profile. This can be explained by looking at the profiles of the tyres where the the generic tyre is slightly wider and with a sharper edge, shown in figure 2.3.

The absolute difference between slick Generic and production tyre profiles was tested over two rims giving consistent results shown in table 3.3

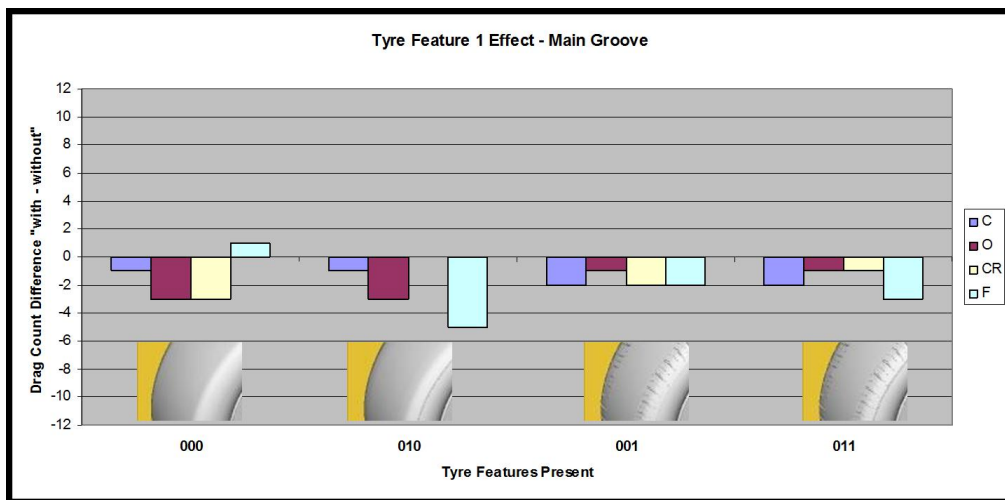
Slick Rim Config.	Tyre 1 - Generic	
	Drag	Lift
Creon	-2	-17
Oden	-2	-15

**Table 3.3:** All values are count differences between slick Tyre 1 and Generic profiles

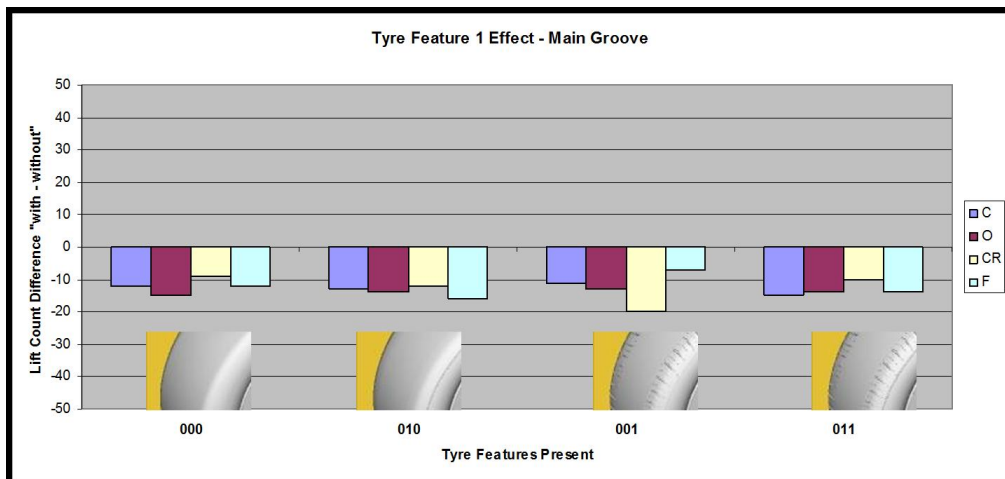
### 3.3 Tyre features

#### 3.3.1 Main Grooves

Figure 3.4 summarizes the results of adding the main grooves on different tyre pattern configurations. As shown adding the main grooves resulted in a slight decrease in drag and a decrease in lift due to the fact that the grooves connect the high pressure region in front of the tyre and low pressure region behind the tyre. This suppresses the jetting effect around the tyre and creates a low pressure region inside the grooves as the flow accelerates through. This matches with previous similar investigations [3, 4, 5]. The lift decrease was mostly between 10 and 15 counts.



(a) Drag count differences



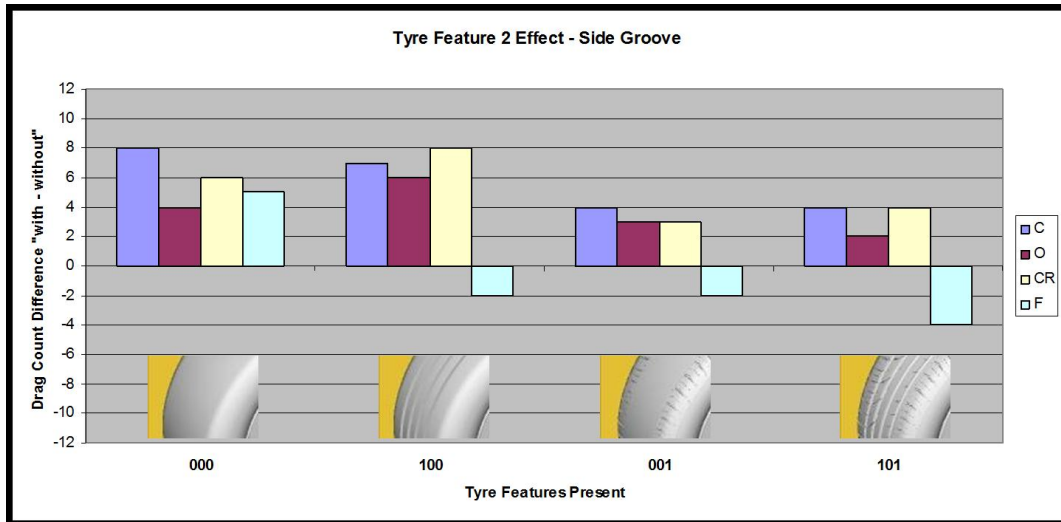
(b) Lift count differences

**Figure 3.4:** Change in aerodynamic forces when main grooves are added on a tyre

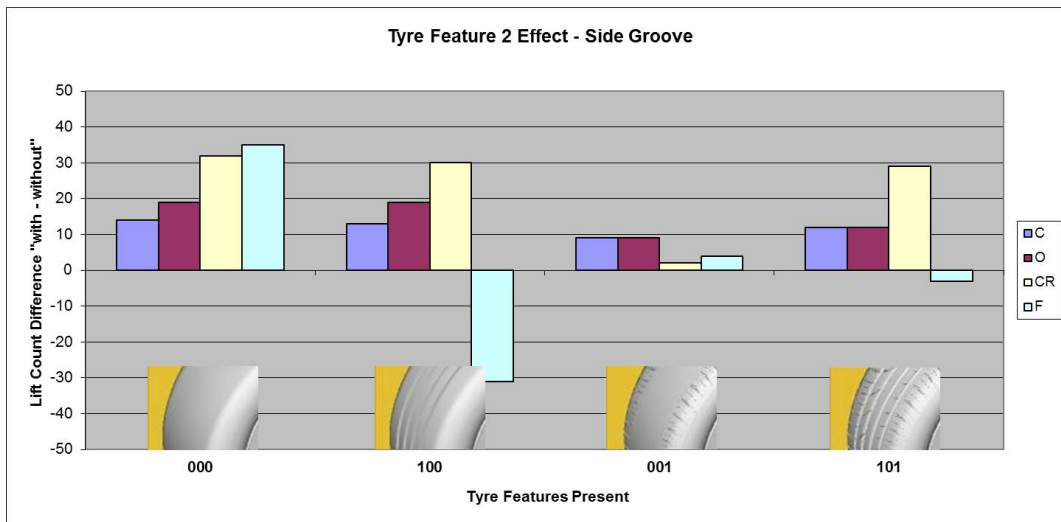
### 3.3. TYRE FEATURES

#### 3.3.2 Side Grooves

Figure 3.5 summarizes the results of adding side grooves on different tyre pattern configurations. As shown in figure 3.5(a) adding the side grooves led to an increase in drag in all simulations where the flow was going through the rim. The flat rim simulations did not show the same trend, except for the slick. The variations in lift can be related to the separation of the flow due to the side groove however no clear trend can be seen.



(a) Drag count differences

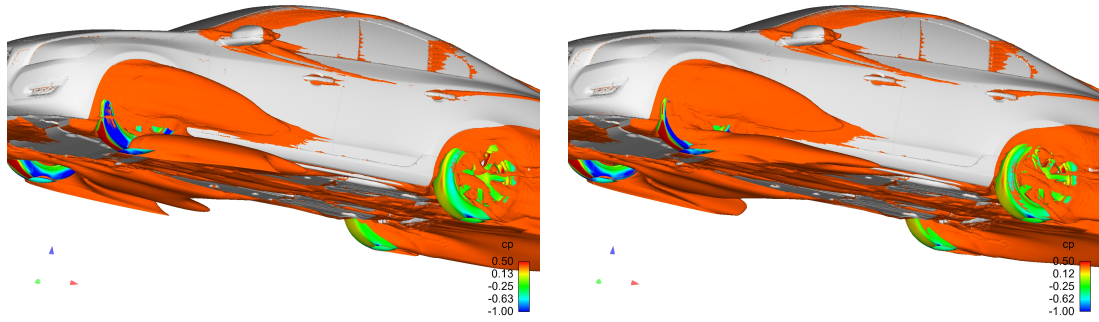


(b) Lift count differences

**Figure 3.5:** Change in aerodynamic forces when side grooves are added on a tyre

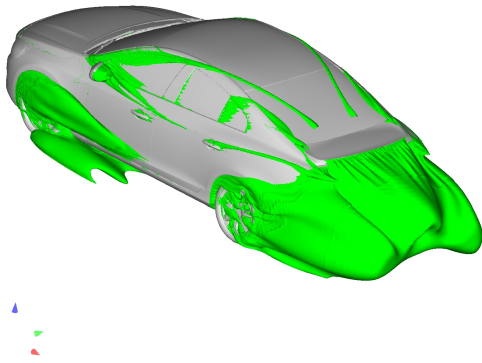
### 3.3. TYRE FEATURES

The biggest difference the side grooves introduced was a clear separation of the flow on the front wheel this changes can be seen in figures 3.6(a) and 3.6(b) . The main drag increase was in most cases accompanied with an increase of the front wheel drag. Figures 3.6(c) and 3.6(d) show that no noticeable change is visible on the rear wake.

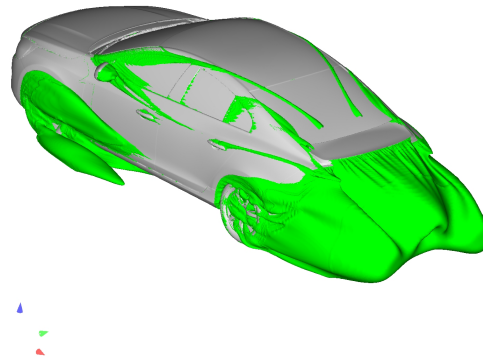


(a) Isosurface  $c_{ptot}=0$  with pressure distribution on wheels for 000

(b) Isosurface  $c_{ptot}=0$  with pressure distribution on wheels for 010



(c) Isosurface  $c_{ptot}=0$  for 000



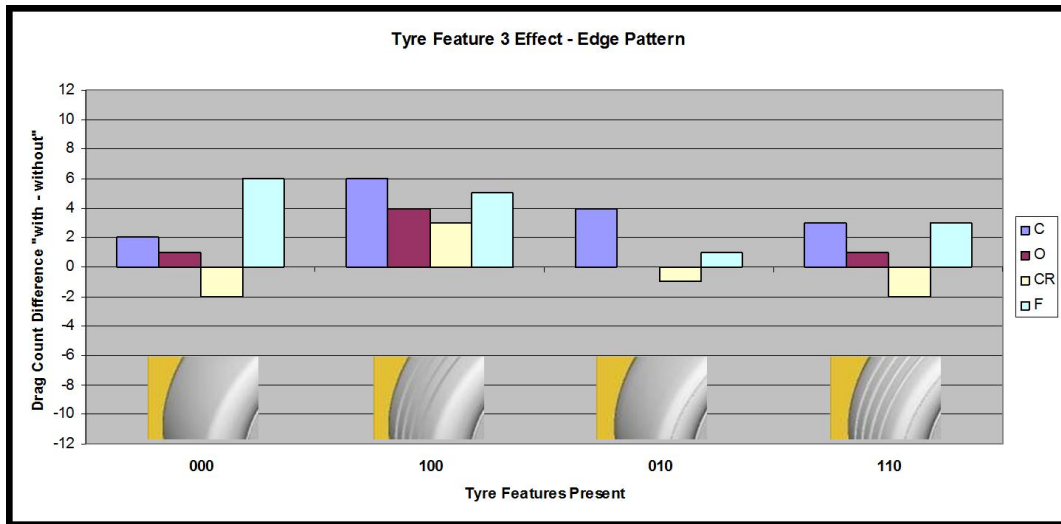
(d) Isosurface  $c_{ptot}=0$  for 010

**Figure 3.6:** Comparison of wake structures of a slick tyre with and without a side groove

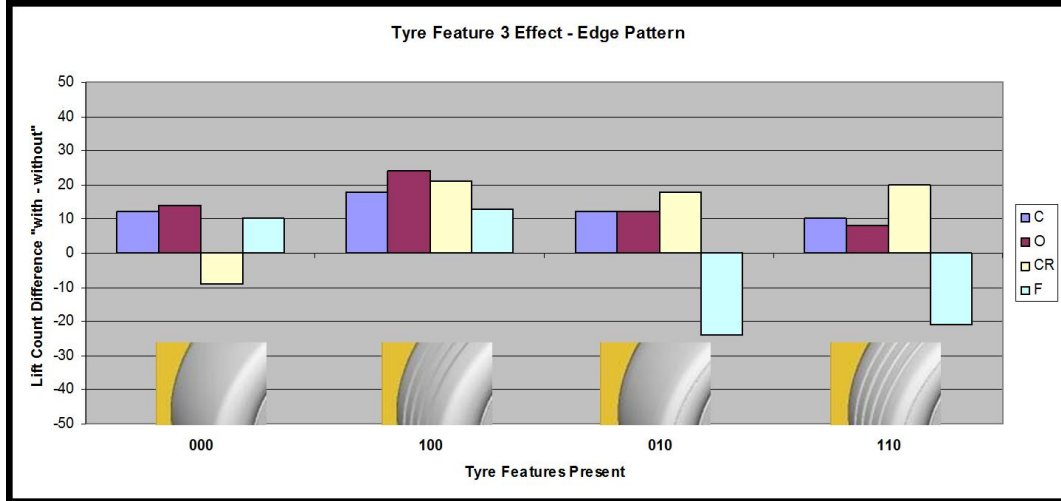
### 3.3. TYRE FEATURES

#### 3.3.3 Edge Pattern

Figure 3.7 summarizes the results of adding the edge pattern on different tyre pattern configurations. No clear trend can be observed due to the presence of a strong interaction with the other tyre features and rim designs. This interaction will be elaborated on later in section 3.3.6



(a) Drag count differences



(b) Lift count differences

**Figure 3.7:** Change in aerodynamic forces when the edge pattern is added on a tyre

### 3.3. TYRE FEATURES

The edge pattern introduced vortices into the flow at the front wheels while also showing a drop in rear base pressure. Its location on the edge of the tread witnesses a flow acceleration as the air moves around the tyre. This along with its rough geometry adds vortices into the flow which can be seen in pictures of flow vorticity around the x axis. Physically this vorticity would represent a swirl in the flow in the x-y plane and propagating downstream along the x-direction. Note: this does not mean that the vortex axis is perfectly parallel to the x axis but it is expected to move downstream. When looking at the drag contribution by parts the rear of the car seemed to have the biggest contribution to the drag increase which can also be seen in the base pressure plots. However the effect of drag increase in some cases has been overcome by a drop in drag on engine bay area or underbody area. This explains some of the non-existence of a well defined trend in the total drag results.

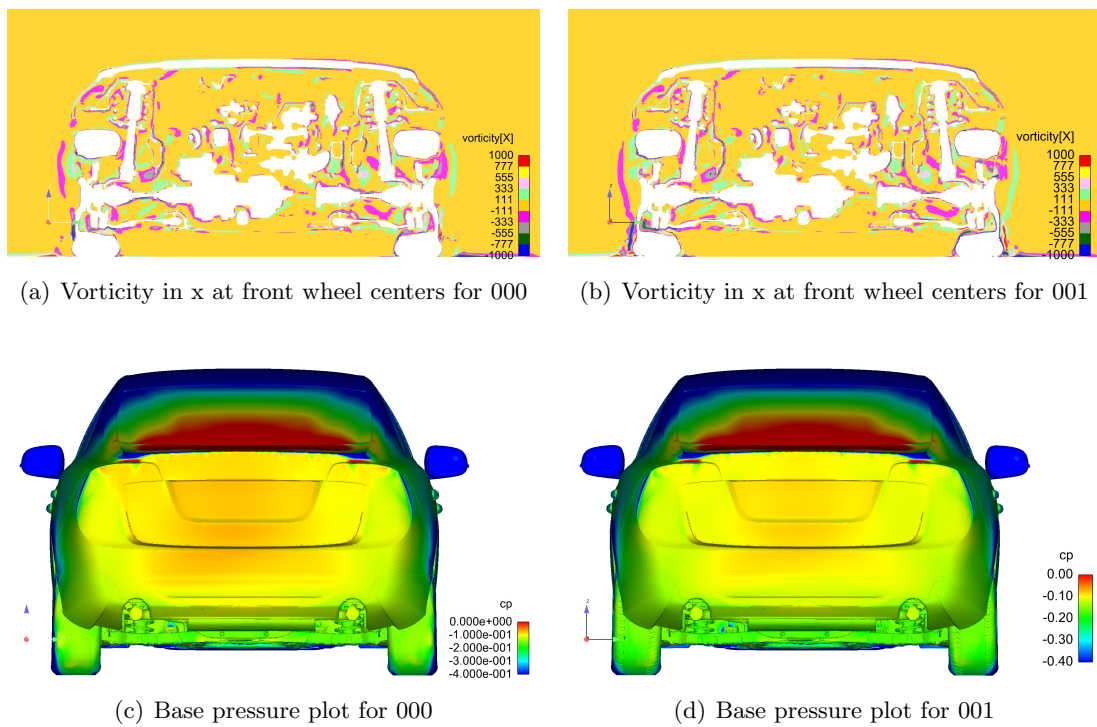
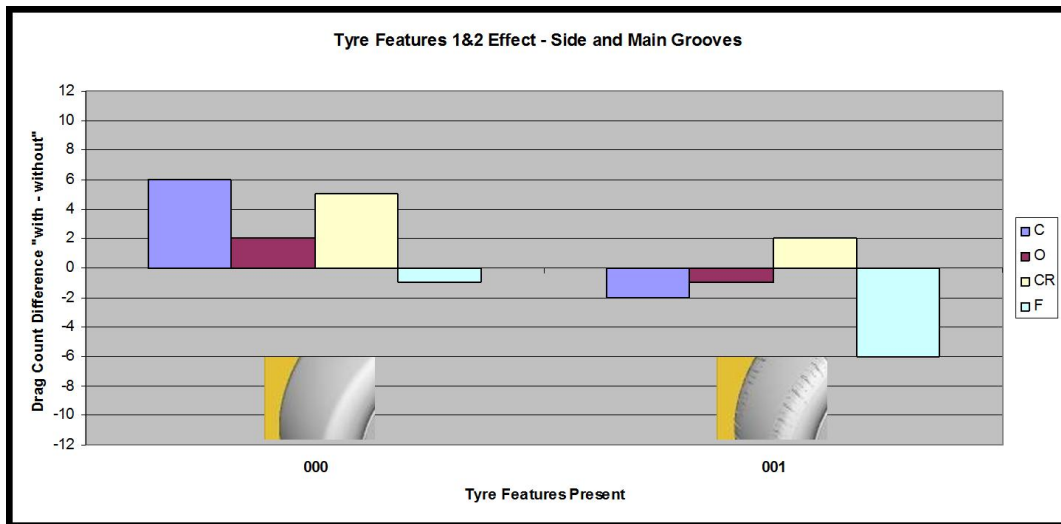


**Figure 3.8:** Comparison of different variables with and without the edge pattern

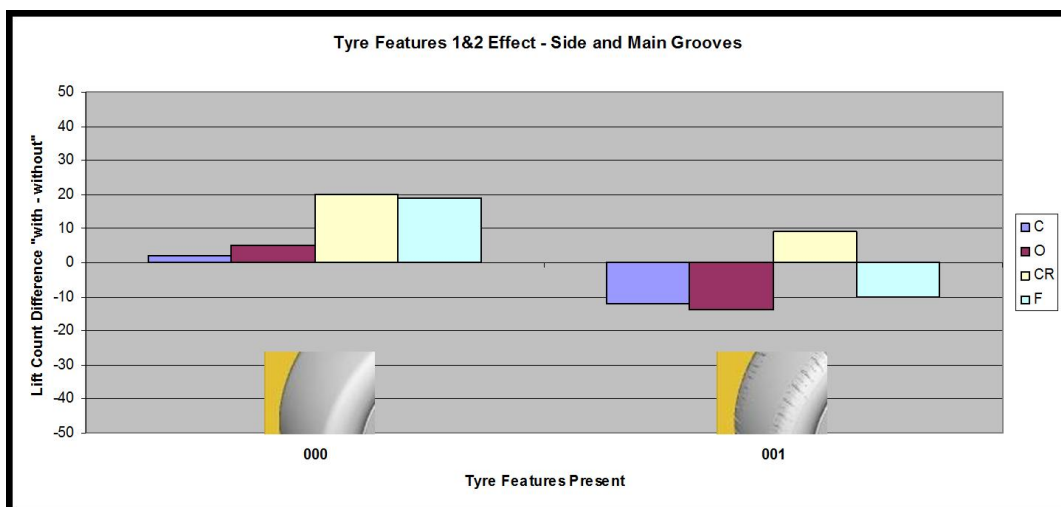
### 3.3. TYRE FEATURES

#### 3.3.4 Main and Side Grooves

Figure 3.9 summarizes the results of adding both the main and side grooves on different tyre pattern configurations. No clear trend can be observed due to the presence of a strong interaction with the other tyre features and rim designs.



(a) Drag count differences



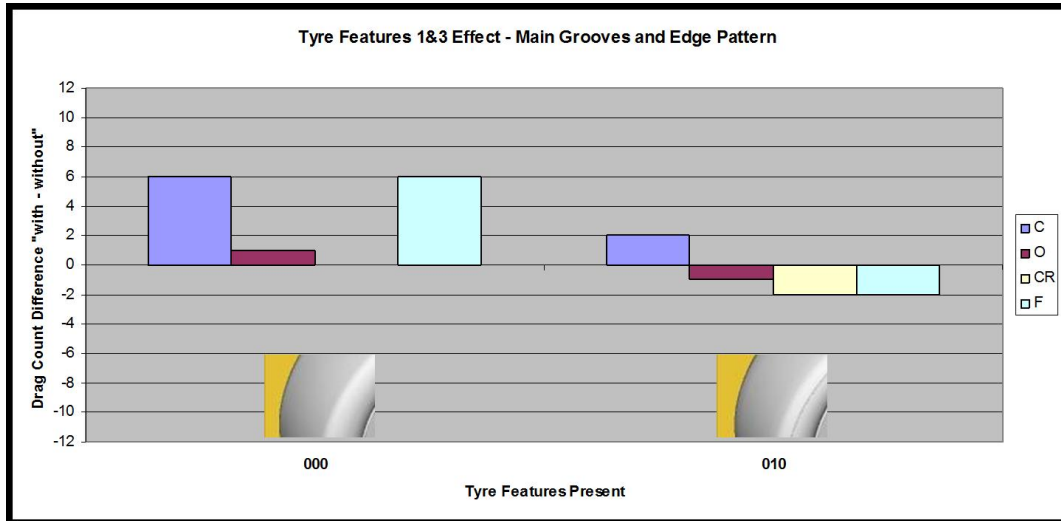
(b) Lift count differences

**Figure 3.9:** Change in aerodynamic forces when the main and side grooves are added on a tyre

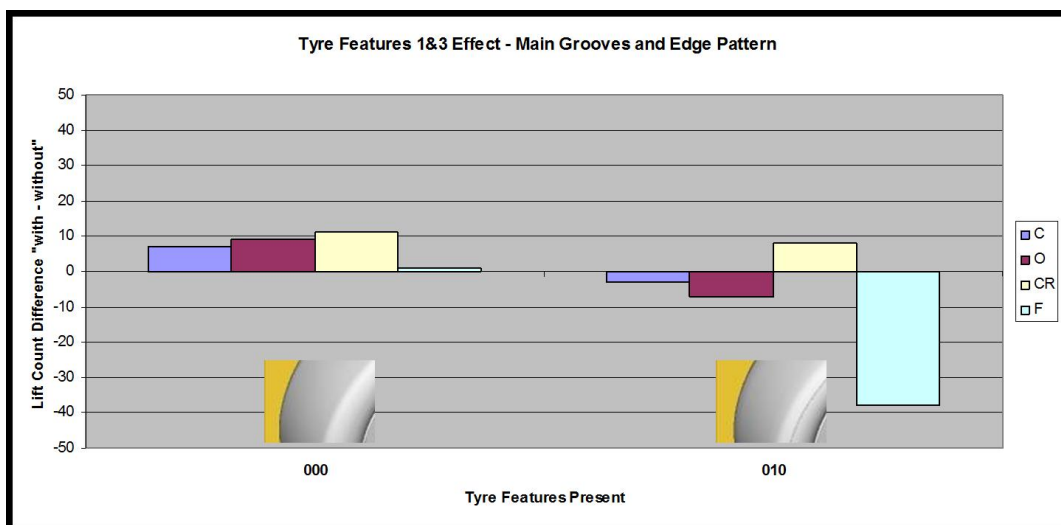
### 3.3. TYRE FEATURES

#### 3.3.5 Main Grooves and edge pattern

Figure 3.10 summarizes the results of adding both the main grooves and edge pattern on different tyre pattern configurations. No clear trend can be observed due to the presence of a strong interaction with the other tyre features and rim designs.



(a) Drag count differences

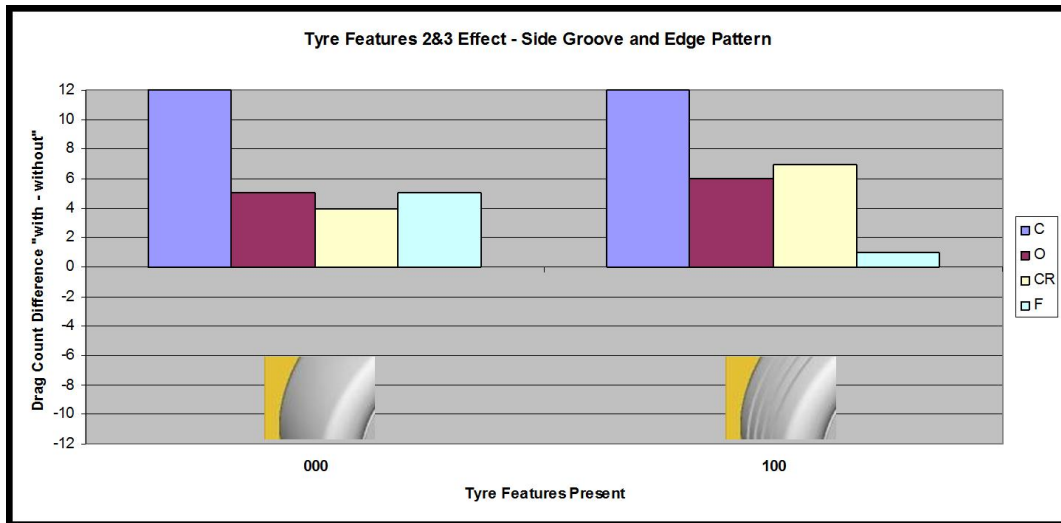


(b) Lift count differences

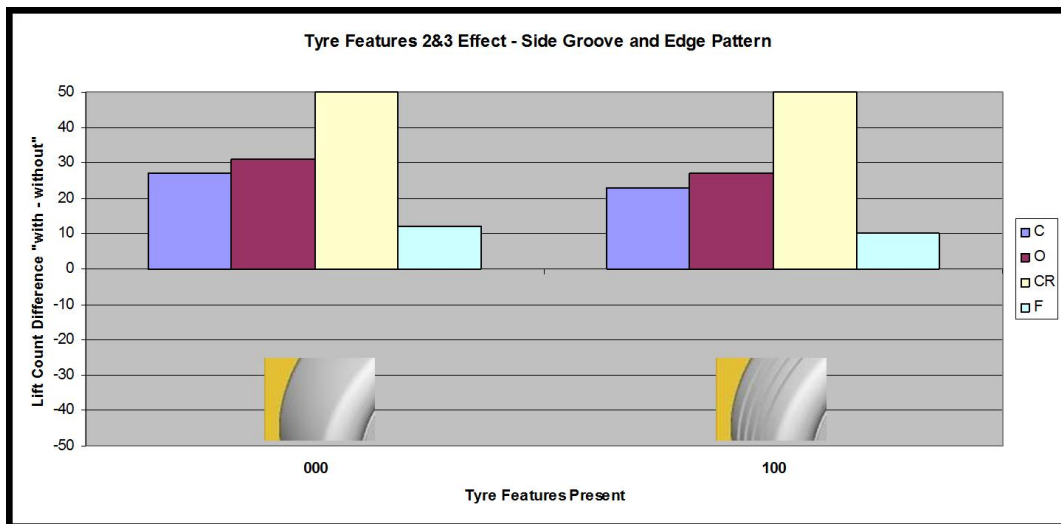
**Figure 3.10:** Change in aerodynamic forces when the main grooves and edge pattern are added on a tyre

### 3.3.6 Side Grooves and edge pattern

Figure 3.11 summarizes the results of adding both the side grooves and edge pattern on different tyre pattern configurations. The combination of both these features added together shows an increase in both drag and lift for all configurations with the magnitude of that increase being dependent on the rim. This shows the existence of a strong interaction between the side pattern and side grooves which in its turn also interacts with the flow through the rim.



(a) Drag count differences



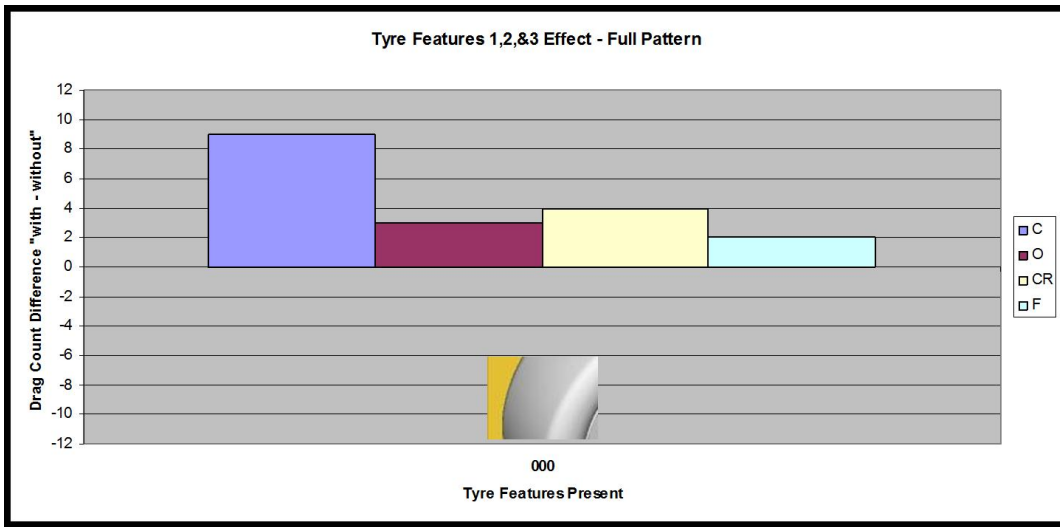
(b) Lift count differences

**Figure 3.11:** Change in aerodynamic forces when the side grooves and edge pattern are added on a tyre

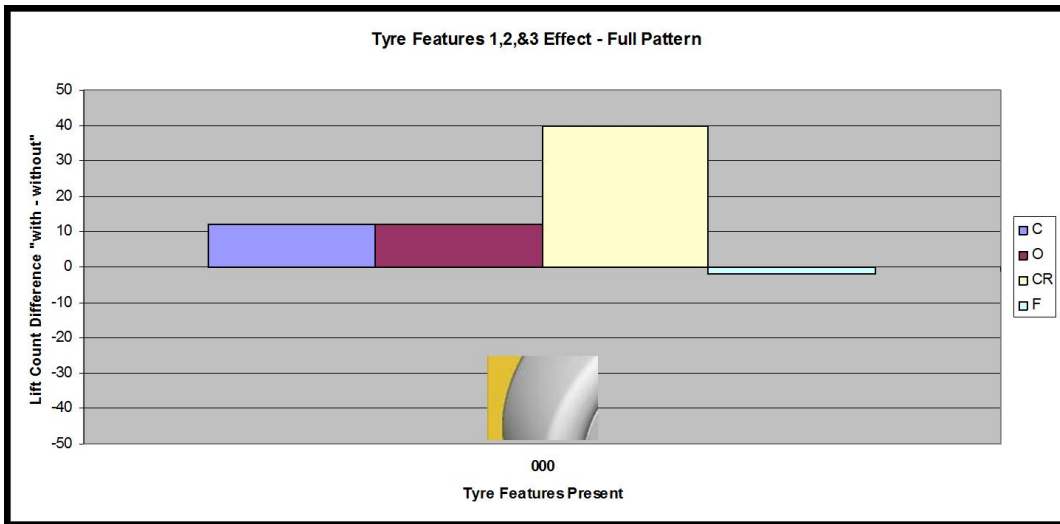
### 3.3. TYRE FEATURES

#### 3.3.7 Full Pattern

Figure 3.12 summarizes the results of adding the full tyre pattern on a slick tyre. Adding the full pattern showed an increase in drag in all cases with the magnitude of the increase being dependent on the rim configuration. The drag differences between slick and pattern tyres were quite visible in the flow field. The contribution from the front wheels can be seen when plotting micro drag, vorticity around x-axis, and separation on the front wheel while the contribution from the rear wheels is more obvious in the rear wake and base pressures.



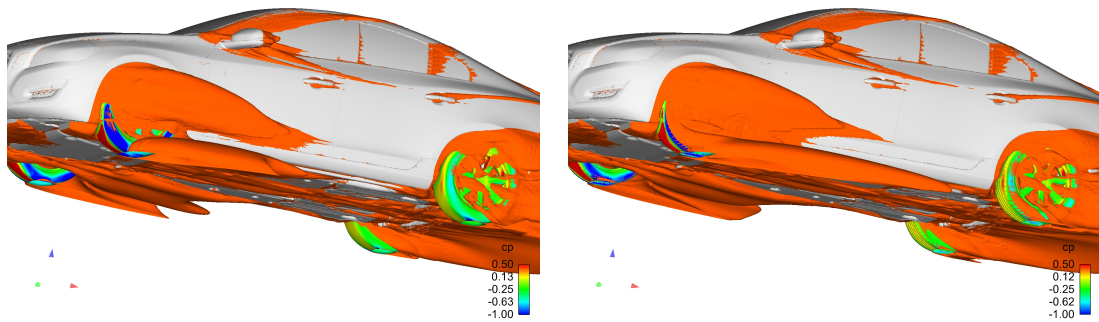
(a) Drag count differences



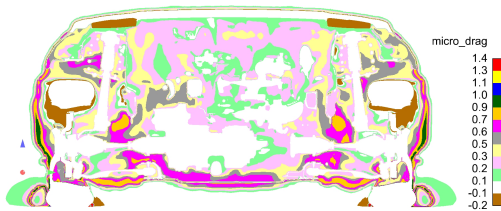
(b) Lift count differences

**Figure 3.12:** Change in aerodynamic forces when the full pattern is added on a tyre

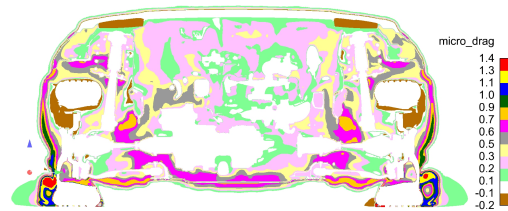
### 3.3. TYRE FEATURES



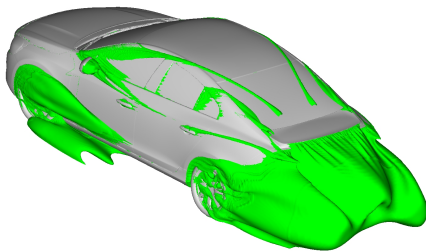
(a) Isosurface  $c_{ptot}=0$  with pressure distribution on wheels for 000 (b) Isosurface  $c_{ptot}=0$  with pressure distribution on wheels for 111



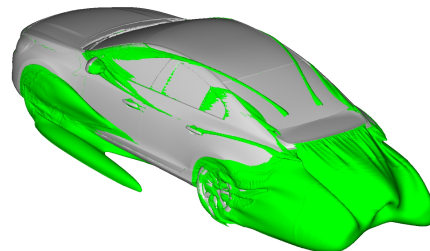
(c) Micro drag at front wheel centers for 000



(d) Micro drag at front wheel centers for 111



(e) Isosurface  $c_{ptot}=0$  for 000



(f) Isosurface  $c_{ptot}=0$  for 111

**Figure 3.13:** Comparison of different variables of a slick tyre and a full pattern tyre

### 3.3. TYRE FEATURES

In previous work by Landström and Sebben [8], wake measurements were done in a plane 500mm rearwards of the front wheel. The test setup included an Oden rim with T1 tyres on a similar sedan vehicle, although the car in the wind tunnel had a different engine than the one in CFD. Figure 3.14 shows how similar the flow field looks like with a full pattern vs how different it is with a slick tyre. Notice how in figure 3.14(c) the two wakes are now connected when a full pattern is introduced unlike the separated wakes when a slick tyre is used, figure 3.14(b). This separation is attributed to the edge pattern and side groove presence. Keep in mind that the measured values are time averaged thus taking into account all spoke positions while the CFD results are all at the same spoke position.

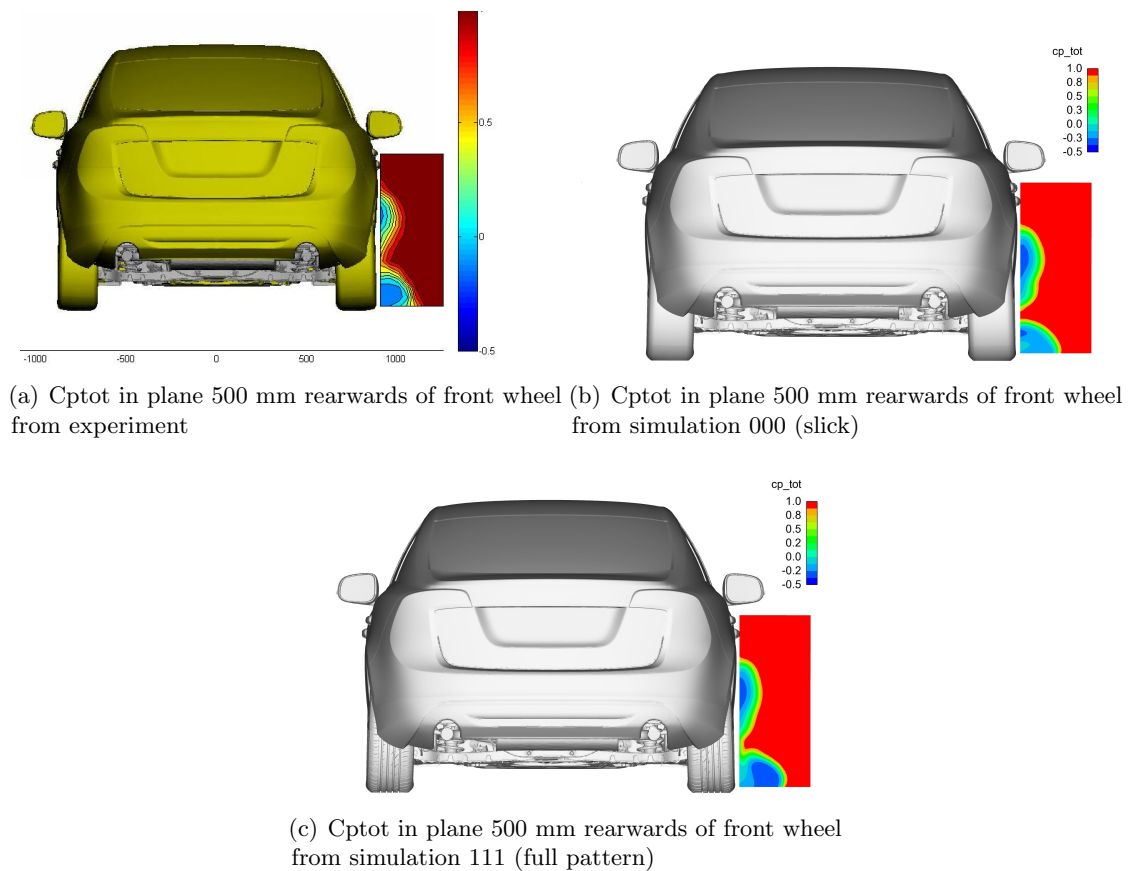
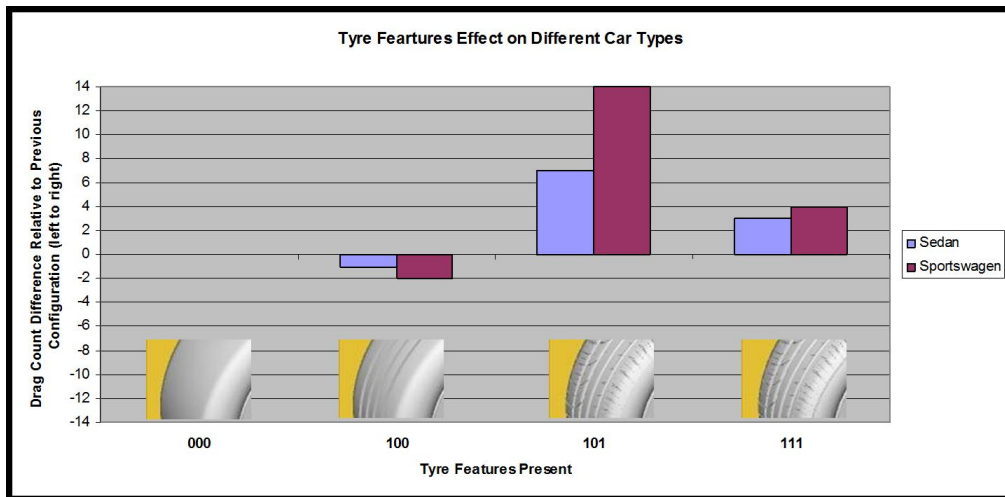


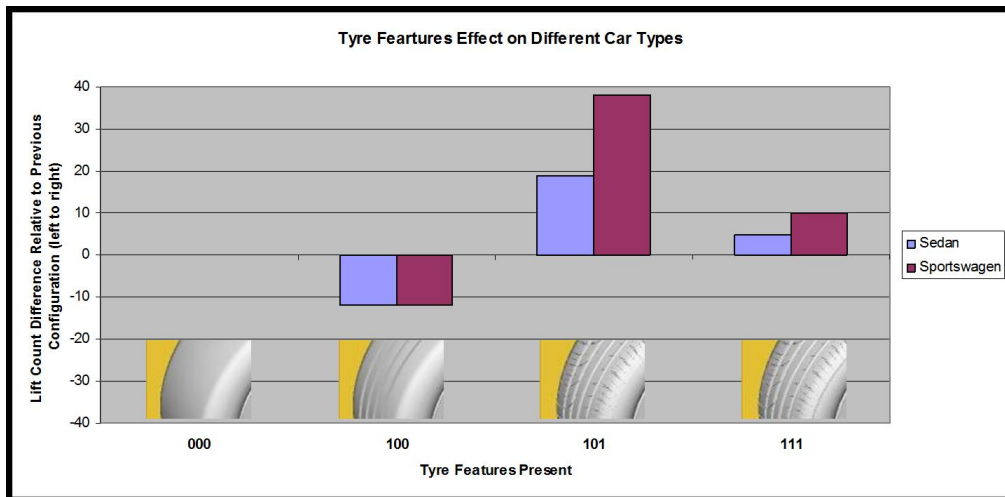
**Figure 3.14:** Comparison of flow structure 500mm rearwards of front wheel between experiment and different simulation configurations

### 3.4 Sedan vs. Sportswagen

In figure 3.15 the Tyre 1 features are added one at a time on the sedan and sportswagen car with Creon rims. The drag difference per step is plotted in the graph. One can notice that the drag and lift increases when the edge pattern is added on the tyre is significantly bigger on the sportswagen than on the sedan car. As this increase did not get canceled out by any other tyre feature, the sportswagen has shown a larger total change from slicks to full pattern tyres.



(a) Drag count differences



(b) Lift count differences

**Figure 3.15:** Change in aerodynamic forces when the pattern features are added consecutively. The plotted values are the difference to the previous configuration going from left to right.

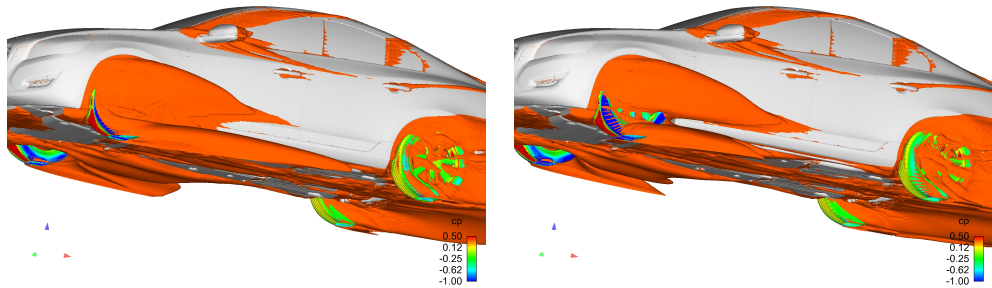
### 3.5 T1 vs. T2

Table 3.4 summarizes the results from the simulations, performed with Tyre 1 and Tyre 2. T2 showed a consistent reduction in drag for all configurations with the magnitude of the reduction being rim dependent. It is worth noting that windtunnel tests on a similar car have shown a similar change in drag on the Oden rim where the dependency on spoke position is expected to be lower than that of the Creon rim due its significantly thinner spokes.

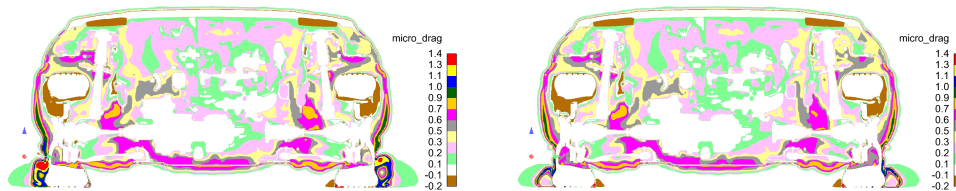
Rim	Drag	Lift
Oden	-4	0
Creon	-1	4
Creon Rotated	-11	-32

**Table 3.4:** All values are count differences to T1

As both tyres have almost identical profiles and main grooves, the reduction in drag can be related to the absence of the side groove on the T2 tyre and the smoother edge pattern. This conforms with the results mentioned previously on the effect of these features.



(a) Isosurface  $c_{ptot}=0$  with pressure distribution on wheels for T1 (b) Isosurface  $c_{ptot}=0$  with pressure distribution on wheels for T2

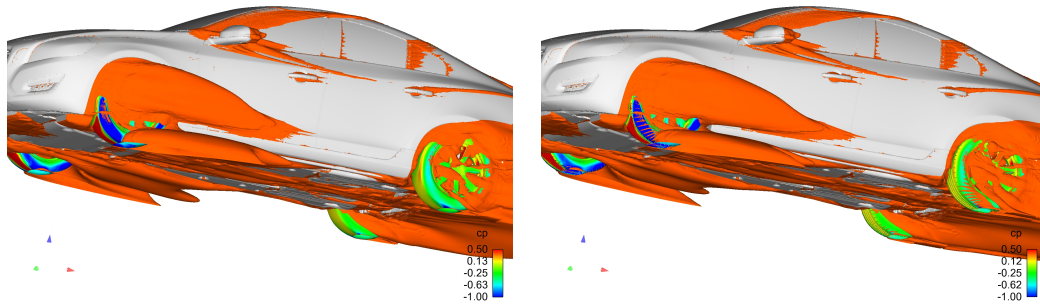


(c) Micro drag at front wheel centers for T1 (d) Micro drag at front wheel centers for T2

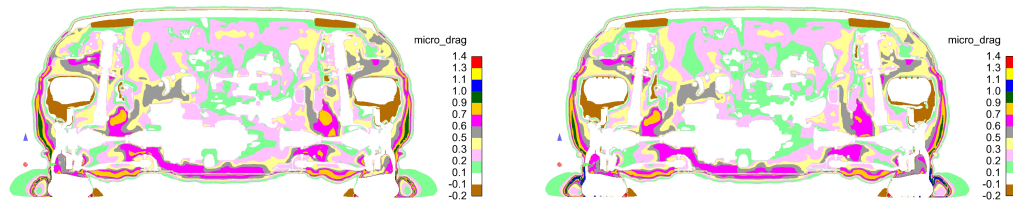
**Figure 3.16:** Comparison of different variables of T1 and T2 simulations

### 3.5. T1 VS. T2

It is also worth noting that Tyre 2 seems to produce very similar flow field to the one produced by a slick tyre. It seems that the main grooves are suppressing the vortices generated by the edge pattern. Keep in mind that this tyre has a smoother edge pattern than Tyre 1 and no side groove. Figure 3.17 shows how similar the flow field looks like and notice how the edge pattern in the absence of the groove contributes to very little increase in local drag.



(a) Isosurface  $c_{ptot}=0$  with pressure distribution on wheels for Slick (b) Isosurface  $c_{ptot}=0$  with pressure distribution on wheels for T2



(c) Micro drag at front wheel centers for Slick (d) Micro drag at front wheel centers for T2

**Figure 3.17:** Comparison of different variables of Slick and T2 simulations

# 4

## Summary

**T**his chapter presents a summary of the limitations and results. First a summary of the encountered limitations is described and keeping these in mind a few conclusions can be made from the present results.

## 4.1 Limitations

The limitations of this work are very similar to usual CFD limitations when it comes to evaluating the effect of small details. The reasons for these limitations can be due to CAD geometry, solver, mesher, VCC CFD procedure, or computational power.

- The most straight forward limitation is the fact that the tyre and rim are not varying in position with respect to time. So the rotation is introduced as a boundary condition instead of a physical mesh rotation and all results are computed for one instance in time. This is due to the high number of CPU hours needed as the current MRF simulations needed 10-12 hours to get results on 204 CPUs. It is also worth mentioning that, the sliding mesh approach cannot be applied on the tyre as it is not circular in shape at ground contact after deforming it under the car's load.
- When applying a rotating moving wall boundary condition all velocities along the cell's normal direction are neglected. Thus a lot of small surfaces inside the tyre blocks did not have a correct boundary condition. this problem is also faced on the faces of the rim spokes however the MRF approach takes care of that problem on the rims thus giving it the correct rotating boundary conditions. However this comes at the expense of a numeric error introduced into the MRF volume in the form of a pressure gradient as the air flow is not always along the wheel's axis of rotation. This error is believed to be insignificant to the flow field distribution.
- Some CAD simplifications had to be introduced on the tyre geometry especially at the contact patch. The most noticeable being that the grooves increase slightly in size and become rectangular in profile. This was a limitation faced in the tyre deformation however in is quite common in CFD to slightly modify geometry for the sake of meshing quality and convergence. In this case this enabled a better mesh which would result in more stable results.
- As standard wall functions were being used one needs to monitor the y-plus distribution. Y-plus values on the car were mostly between 30 and 300 thus meeting the criteria to use the standard wall function. On the tyre itself however, as the mesh was 1.25mm y-plus values dropped till around 12 in few regions especially inside the rubber blocks were the velocity is lower than the outer surface of the tyre. This does not meet the recommendation for standard wall function however switching to non-equilibrium wall function was not going to make a difference as the two-layer approach only changes below y-star of 11.25 where the standard wall function completely deteriorates. Of course this is only considering the validity of these functions relative to the mesh and not comparing their performance in accounting for pressure recovery and steep pressure gradients. The standard wall function is the standard function and VCC and have shown to be stable.
- Mesh dependency is one of the most common problems in CFD simulations. In all above simulations the same mesh setting were preserved. However when certain

tyre features need were removed then it is natural that the mesh would be slightly different in that region. In the last phase of this thesis a small investigation was run on that and showed a noticeable change in absolute value however this does not necessarily mean that the difference between the configurations would not be different as well. Further investigation on that issue is needed.

## 4.2 Conclusions

That being said, a few conclusions can be made based on the differences between the different configurations.

- Main grooves: the main grooves have shown consistent results of drag and lift reduction when connected through beneath the tyre using def2. No big changes could be seen on the flow field though.
- Side grooves: the side groove have shown to trigger flow separation and resulting in drag increase, especially at the front wheels. However, more investigation on the matter is needed and a more thorough evaluation of mesh dependency should be performed on such small features.
- Edge pattern: the edge pattern have shown to introduce a high vorticity in the flow. As the flow passes around the tyre a vortex seems to be generated at the edge pattern as the flow is accelerating over the rough tyre edge. The interaction between the edge pattern and the flow showed an influence in the rear wake which was also visible in base pressure plots.
- A strong interaction between the tyre and the rim can be seen where the magnitude of the drag changes in several cases was dependent on the rim design or the spoke position of the same rim. Aerodynamic optimization of both should go hand in hand and optimization of either should take into consideration a reasonable sample of the other, i.e if a certain tyre is to be optimized it should be done on a small sample of different rims at the same time.
- Tyre 2 has shown lower drag figures than Tyre 1 in CFD. However only one of these cases has been tested in windtunnel on an Oden rim showing similar results. The main reason for the decrease in drag can be attributed to a smoother edge pattern and the absence of a side groove.
- Tyre pattern has shown a higher influence on a vehicle drag on a sportswagen than on a sedan. The interaction of the tyre with the flow seems to have a bigger effect when the rear wake is bigger. The major contribution is believed to be from the edge pattern on the rear wheels.

### 4.3 Recommendations

A few recommendations come to mind on modeling tyres in CFD simulations

- Accurately replicate tyre deformation under loading and rotation while preserving tyre pattern features at contact patch.
- Use real tyre profiles for slick tyres as it represents the real life geometry more closely. For the cases investigated the real tyre profile has shown a slight drop in drag and a significant drop in lift compared to Generic tyres.
- Use slick tyres with correct tyre profiles in CFD simulations as a full pattern tyre with good aerodynamics is expected to give similar results.
- Try to have a rim with small spokes to eliminate the dependency of the simulations on the spoke position when running computations using MRF approach. A rim significantly bigger than the brake disc would help as well as it reduces the blockage effect of the brakes and suspension components. It allows more flow through thus helps to neutralize the spoke position dependency.
- When doing rim optimization, a fully detailed tyre should be used with transient sliding mesh simulations to eliminated spoke dependency and capture the tyre-rim interaction.

### 4.4 Future Work

- Investigate the mesh dependency of such simulations when it comes to such tiny details as a tyre pattern
- Investigate effect of tyre pattern on vehicle optimization such as :front bumper, front wheel deflectors, rear bumper, underbody panels, etc...
- Perform wind tunnel tests with physical tyres representing similar tyre feature configurations to confirm the numerical results.

# Bibliography

- [1] C. Mercker, N. Breuer, H. Berneburg, H. Emmeltman, *On the Aerodynamics Interference Due to Rolling Wheels of Passenger Cars*, SAE Technical Paper, 1991, 1991-910311.
- [2] C. Landström, S. Sebben, L. Löfdahl, *Effects of Wheel Orientation on Predicted Flow Field and Forces When Modeling Rotating Wheels Usind CFD*, 8th Mira International Conference on Vehicle Aerodynamics, 2010, ISBN: 978-1-906400-08-8.
- [3] I. Dimitriou, S. Klussmann, *Aerodynamic Forces of Exposed and Enclosed Rotating Wheels as an Example of the Synergy in the Development of Racing and Passenger Cars*, SAE Technical Paper, 2006, 2006-01-0805.
- [4] J. Fackrell, J. Harvey, *The Aerodynamics of an Isolated Road Wheel*, AIAA 2nd Symposium on Aerodynamics and Competition Automobiles, Volume 16, Pages 119-125, May 11, 1974, Los Angeles, California.
- [5] A. Mears, R. Dominy, D. Sims-Williams, *The Air Flow About an Exposed Racing Wheel*, SAE Technical Paper, 2002, 2002-12-02.
- [6] E. Mercker, H. Berneburg, *On the Simulation of Road Driving of a Passenger Car in a Wind Tunnel Using a Moving Belt and Rotating Wheels*, 3rd International Conference Innovation and Reliability, Florence, Italy, April 8-10, 1992.
- [7] C. Landström, L. Josefsson, L. Löfdahl, T. Walker, *Aerodynamic Effects of Different Tyre Models on a Sedan Type Passenger Car*, SAE World Congress, 2012, 2012-04-16.
- [8] S. Sebben, C. Landström, *Prediction of Aerodynamic Drag for Different Rim Designs Using Varied Wheel Modelling in CFD*, 8th FKFS Conference - Progress in Vehicle Aerodynamics and Thermal Managment, 2011.
- [9] Q. Zhiling, *Wheel Aerodynamic Developments by Module-Based Prototype Rims and Stationary Rim Shields*, FISITA World Automotive Congress 2010, Budapest Hungary, Volume 1, Page 1698, FISITA2010B034, ISBN: 978-1-61784-507-1.

- [10] S. Sebben, P. Mlinaric, *Investigation of the influence of Tyre Deflection and Tyre Contact Patch on CFD Predictions of Aerodynamic Forces on a Passenger Car*, 7th Mira International Vehicle Aerodynamics Conference, 22-23 October, Warwickshire, UK, 2008.
- [11] L. Sterken, *Numerical Investigation of Passenger Car Aerodynamics Method Optimization and Experimental Correlation*, Master's Thesis, Technical University Delft, 2009.